Supporting Information

Acidity/Reducibility Dual-Responsive Hollow Mesoporous Organosilica Nanoplatforms for Tumor-Specific Self-Assembly and Synergistic Therapy

Wei Tang,[†] Wenpei Fan,[†,] Zhantong Wang,[†] Weizhong Zhang,[‡] Shiyi Zhou,[‡] Yijing Liu,[†] Zhen Yang,[†] Emily Shao,[†] Guofeng Zhang,[§] Orit Jacobson,[†] Lingling Shan,[†] Rui Tian,[†] Siyuan Cheng,[†] Lisen Lin,[†] Yulun Dai,[†] Zheyu Shen,[†] Gang Niu,[†] Jin Xie,[‡,*] Xiaoyuan Chen[†,*]*

† Laboratory of Molecular Imaging and Nanomedicine (LOMIN), National Institute of Biomedical Imaging and Bioengineering (NIBIB), National Institutes of Health (NIH), Bethesda, Maryland 20892, United States

‡ Department of Chemistry, University of Georgia, Athens, Georgia 30602 United States

§ Laboratory of Cellular Imaging and Macromolecular Biophysics, National Institute of Biomedical Imaging and Bioengineering (NIBIB), National Institutes of Health (NIH), Bethesda, Maryland 20892, United States

*E-mail: wenpei.fan@nih.gov, jinxie@uga.edu, shawn.chen@nih.gov

Part A: Experimental Section

Synthesis of HMSN. Inorganic hollow-structured mesoporous silica nanoparticles (HMSNs) were synthesized according to a typical "structural difference-based selective etching" strategy. First, 74 mL of ethanol, 10 mL of ultrapure water, and 3.14 mL of ammonia solution were mixed and vigorously stirred at 30 °C, followed by addition of 6 mL of TEOS. After 1 h of reaction, the resulting SiO_2 nanoparticles were obtained by centrifugation, washed with ethanol for two times and then dispersed in 60 mL of ultrapure water. Second, CTAC was used as pore-forming agents for mesoporous silica coating on SiO_2 nanoparticles. 2 g of CTAC and 0.04 g of TEA were mixed in 20 mL of ultrapure water, followed by addition of 10 mL of the above as-synthesized SiO_2 nanoparticles. After 1 h of stirring, the system was transferred to an 80 °C oil bath, followed by dropwise addition of 0.6 mL of TEOS. After 1 h of reaction, the resulting SiO_2@MSN particles were centrifugated and washed with ethanol for two times, and finally dispersed in 30 mL of ultrapure water. Third, Na_2CO_3 was used to fabricate the cavity by selectively etching away the internal SiO_2 core. 0.6 M Na_2CO_3 was added to 30 mL of the above SiO_2@MSN solution, and then the system was transferred to an 80 °C oil bath for 1 h of reaction. Afterwards, the resulting HMSN particles were obtained by centrifugation and washed with ultrapure water for two times. The CTAC template of HMSNs were extracted with NaCl in 30 mL of methanol (1 wt.%) at room temperature. The extraction was repeated for several times to completely remove the CTAC, and the final HMSN products were dispersed in ultrapure water.

Synthesis of Mo(VI)-Based POM. The Mo-based POM clusters with the highest oxidation state of Mo(VI) were synthesized *via* a one-pot approach. 10 mL of 2 mmol of $(NH4)_6Mo_7O_{24}\cdot 4H_2O$ and 5mL of 1.17 mmol of $NaH_2PO_4\cdot 2H_2O$ were reacted in ultrapure water for 15 min. Next, 80

mL of ethanol was added to terminate the reaction. Finally, the resulting *Ox*-POM clusters were collected, washed with water and ethanol for three times, and finally freeze-dried for further use.

Blood Hemolysis. Mice whole blood was collected. Red blood cells (RBCs) were separated from the whole blood by centrifugation at 2000 rpm/min for 10 min and were washed with PBS for three times for further evaluations. The RBCs were aliquoted and resuspended in 1 mL of different thioether/phenylene dual-hybridized HMON/PBS solutions at concentrations ranging from 16.625 – 1000 μg/mL. For controls, two RBC aliquots were suspended in 1 mL of PBS (negative control) and ultrapure water (positive control), respectively. The above mixtures were incubated at room temperature for 2 hours. After the incubation, the supernatants were collected, and the UV-Vis absorbance spectra were recorded. The hemolytic percentage was calculated based on the following equation: Hemolysis% = $(A_{HMONs} - A_{(-)control}) / (A_{(+)control} - A_{(-)control})$, where A is the absorbance at λ = 541 nm. For comparison, the hemolytic effect of traditional HMSNs was also evaluated.

***In Vitro* Photothermal Heating.** To evaluate the self-adaptive photothermal conversion, HMOPM solutions at various GSH concentrations (0, 2, 5, 10, 20 mM) and at different pH values (7.4, 6.5, 5.5) were irradiated with an 808-nm laser at 1.0 W/cm^2 for 5 minutes. In a separate study, to investigate the irradiation dose-dependent photothermal effect, HMOPM-CO solutions at pH= 7.4 and GSH concentration of 10 mM were irradiated with an 808-nm laser at different irradiation fluence (0.3, 0.5, 1.0 W/cm^2) for 20 min. A SC300 infrared camera was employed to record thermal images and measure the temperature of the solutions during the irradiation.

***In Vitro* PA imaging.** HMOPM solutions at various GSH concentrations (0, 2, 5, 10, 20 mM) and at different pH values (7.4, 6.5, 5.5) were filled into polyethylene 50 capillaries. The capillaries were positioned in a water bath and imaged from the top using a 40 MHz, 256-element linear array

transducer with a Visual Sonic Vevo 2100 LAZR system. The PA signals were quantified as the average pixel intensities according to the region of interests (ROIs).

Cell Line and Animal Models. The U87MG human glioblastoma cell line was obtained from the American Type Culture Collection and cultured with Dulbecco's Modified Eagle Medium in a cell culture flask. Athymic nude mice and Balb/c mice were purchased from Envigo laboratories. The animal model was established by subcutaneously injecting around 3×10^6 U87MG cells into the right front limb of each athymic nude mouse. All the experimental procedures had been conducted by following a protocol approved by the animal care and use committee (ACUC) of the National Institutes of Health Clinical Center (NIHCC).

MTT Assay. Around 1×10^4 U87MG cells were seeded in each well of a 96-well plate and incubated overnight. To evaluate the biocompatibility, POMs, HMONs, HMOPMs, and HMOPMs-CO at different concentrations were added to the plate in separate groups. After 24 hours of incubation, the cells were washed and replenished with 80 μL of fresh medium and 20 μL of 5 mg/mL MTT (Thiazolyl Blue Tetrazolium Bromide). After another 4 hours of incubation, the medium containing MTT was replaced with 150 μL of DMSO and the absorbance of each well was measured at the wavelength of 490 nm by a microplate reader.

***In Vitro P*hototoxicity.** The HMOPMs and the HMOPMs-CO at a concentration of 1 mg Mo/mL were pre-incubated with 10 mM GSH for 24 hours to serve as stocking solutions. Next, U87MG cells were treated with the GSH pre-incubated HMOPM and HMOPM-CO solutions at the same concentration of 100 μg Mo/mL and then exposed to an 808-nm irradiation at 1.0 W/cm^2 for 5 min or 0.3 W/cm^2 for 20 min. In other control groups, the cells were treated with the HMOPMs-CO only, an 808-nm irradiation at 1.0 W/cm^2 for 5 min only, or PBS only. Subsequently, the cell

culture medium was removed, and the cells were washed twice with PBS and replenished with fresh medium. After incubating for 24 hours, MTT assays and live and dead assay were performed to evaluate the cell viability, and Annexin V-FITC/PI flow cytometry analysis was performed to investigate the cell apoptosis. For the live and dead assay, the cells after 24 hours of the treatment were incubated with calcium AM and PI working solution (Sigma, 04511). After 30 min of the incubation, the cells were washed twice with PBS and observed under a Zeiss LSM 780 confocal microscopy. For the Annexin V-FITC/PI flow cytometry analysis, the cells after 24 hours of the treatment were stained with 5 μL of annexin V- FITC and 10 μL of PI working solutions (BioLegend, 640914) for 15 min at room temperature and were examined by a BD Accuri C6 flow cytometry. In a separate study, to better-evaluate the GSH-activated PTT effect, U87MG cells were treated with HMOPMs-CO and HMOPMs (100 μg Mo/mL) without the GSH preincubation and then exposed to an 808-nm irradiation at 1.0 W/cm^2 for 5 min or 0.3 W/cm^2 for 20 min. Cells treated with PBS plus the two irradiations were also performed as controls. Right after the irradiations, the spent medium was replaced with fresh medium and MTT assays were applied after 24 hours of incubation.

^{64}Cu Labelling. 2 μL of $^{64}CuCl_2$ (3-5 mCi) was added to 0.5 mL of 10 mM MES buffer (pH 7.3). The solution was shortly vortexed and incubated for 1-2 minutes. Thereafter, 0.5 mCi of ^{64}Cu was transferred to a vial containing the HMOPM NPs. The reaction was vortexed and heated to 70 °C for 45-60 minutes. After cooling to ambient temperature, an aliquot was taken for determination of radiochemical purity by radio-TLC using 0.1 M Citric acid (pH 5) as a development solvent. The retention factor (R_f) of ^{64}Cu-HMOPM was ~ 0 - 0.1 and that of free ^{64}Cu was ~ 0.9.

***In Vivo* PA Imaging.** The HMOPMs-CO and the HMOPMs were intravenously injected into U87MG tumor-bearing mice (n=3) at the same dosage of 100 mg Mo/kg in separate groups. The

tumors were imaged with a Visual Sonic Vevo 2100 LAZR system equipped with a 40 MHz, 256-element linear array transducer before and at 2, 4, 8, 24, 48 h post-injection of the two nanoparticles.

HO-1 Staining. 20μm of slides were prepared, fixed with 4% paraformaldehyde, and blocked with 2 % BSA/PBS for 30 min at room temperature. The slides were then stained with a HMOX1 Monoclonal Antibody (HO-1-1) (Invitrogen, Catalog #: MA1-112) at a dilution of 1:200 overnight at 4℃. After washing with PBS, the slides were labeled with an Alexa Fluor 488-conjugated goat anti-mouse IgG (H+L) secondary antibody (Invitrogen, Catalog #: A28175) at a dilution of 1:1000 for 45 min at room temperature and mounted with mounting medium with DAPI (*VECTASHIELD*, Catalog #: H-1200).

TUNEL Assay. 20μm of slides were prepared and fixed with 4% paraformaldehyde in PBS (pH 7.4) for 10 minutes at room temperature. After washing with PBS, the slides were incubated in permeabilization solution (0.1 % Triton X-100, 0.1 % sodium citrate in water, freshly prepared) on ice for two minutes. Then the slides were washed, and the tumor samples were incubated with TUNEL reaction mixture (Roche, catalog #: 6432344001) for 60 minutes at 37 °C in a humidified atmosphere in the dark. After gently rising with PBS, the slides were mounted with mounting medium with DAPI (*VECTASHIELD*, Catalog Number: H-1200) and ready for confocal luminescence imaging.

Characterization. Transmission electron microscopy (TEM) images were acquired on a FEI Tecnai T12 electron microscope. Dynamic light scattering (DLS) data was recorded on a Malvern ZetaSizer Nano instrument. UV–Vis absorption spectrum was recorded by using a Shimadzu UV-2501 spectrophotometer. Fluorescence spectrum was measured on a Hitachi F-7000 fluorescence spectrophotometer. Raman spectrum was acquired on a Thermofisher spectrometer (DXR) with the excitation wavelength of 633 nm. X-ray photoelectron spectroscopic spectrum was tested with

a high sensitivity Kratos AXIS 165 spectrometer. N_2 adsorption−desorption isotherm and corresponding pore size distribution were acquired on a Micrometitics Tristar 3000 system. Photothermal heating images were recorded with a SC300 infrared camera. PA images were acquired with a Visual Sonic Vevo 2100 LAZR system. PET images were performed on a micro Inveon PET scanner (Siemens Healthcare GmbH, Germany). Confocal laser scanning microscopy (CLSM) images were obtained on a Zeiss LSM 780 microscopy. Flow cytometry analysis was performed on a BD Accuri C6 flow cytometry.

Statistical Methods. Quantitative data were expressed as mean ± SD. Means were compared using Student's t-test. $*P < 0.05$, $**P < 0.01$, and $***P < 0.001$ were considered significant, moderately significant, and highly significant, respectively.

Part B: Supplementary Figures

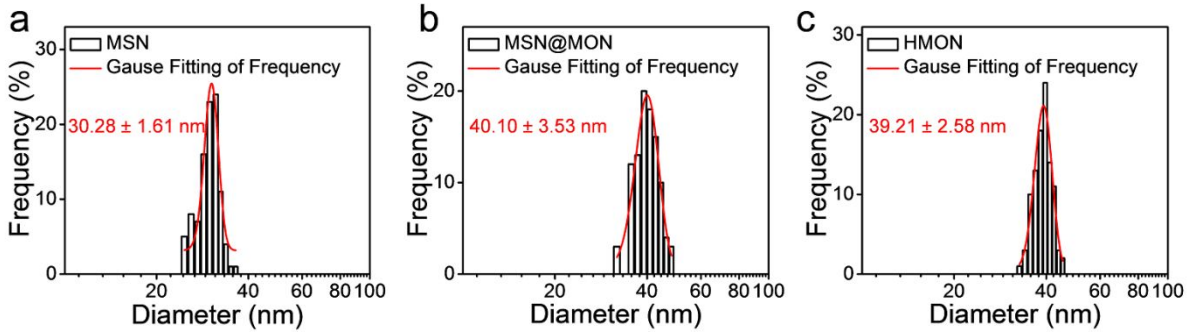

Figure S1. Size distribution analysis of (a) MSN, (b) MSN@MON, and (c) HMON based on the TEM images of Figure 1b, showing an average diameter of 30.28 ± 1.61 nm, 40.10 ± 3.53 nm, and 39.21 ± 2.58 nm, respectively.

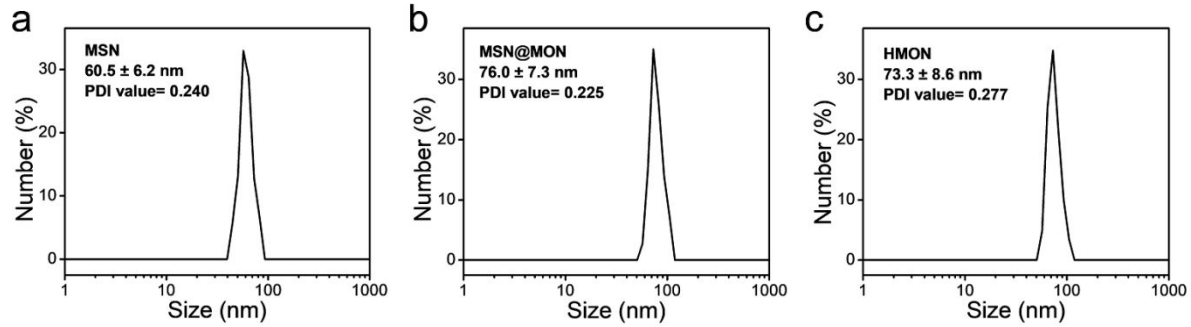

Figure S2. Dynamic light scattering (DLS) size measurements of (a) MSN, (b) MSN@MON, and (c) HMON, showing a hydrodynamic size of 60.5 ± 6.2 nm, 76.0 ± 7.3 nm, and 73.3 ± 8.6 nm, respectively. Their polydispersity indexes were 0.240, 0.225, and 0.277, respectively.

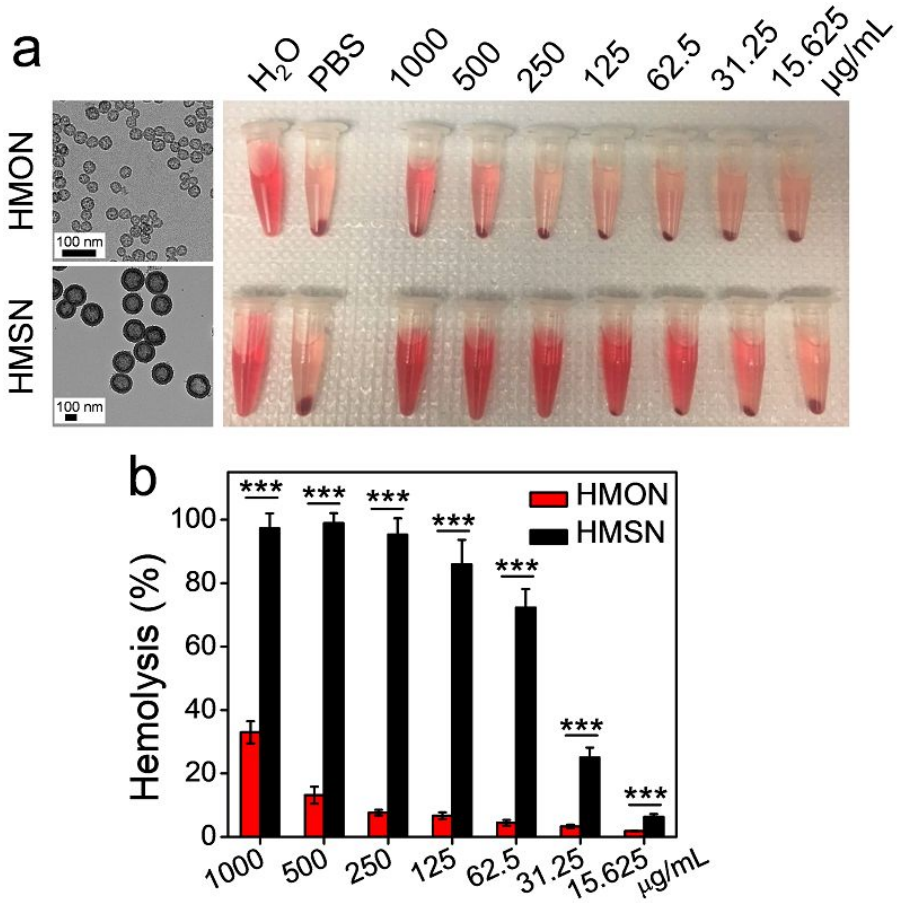

Figure S3. Blood hemolysis analysis of HMON and HMSN. (a) TEM images (scale bar, 100 nm) and photographs of RBCs after co-incubation with HMON and HMSN at different concentrations (15.625, 31.25, 62.5, 125, 250, 500, and 1000 μg/mL). Ultrapure water and PBS were set as positive and negative control, respectively. (b) The calculated hemolytic percentages of RBCs after the co-incubation with HMON or HMSN. The HMON exhibited much lower hemolytic effect than the HMSN at all tested concentrations. *** $P < 0.001$.

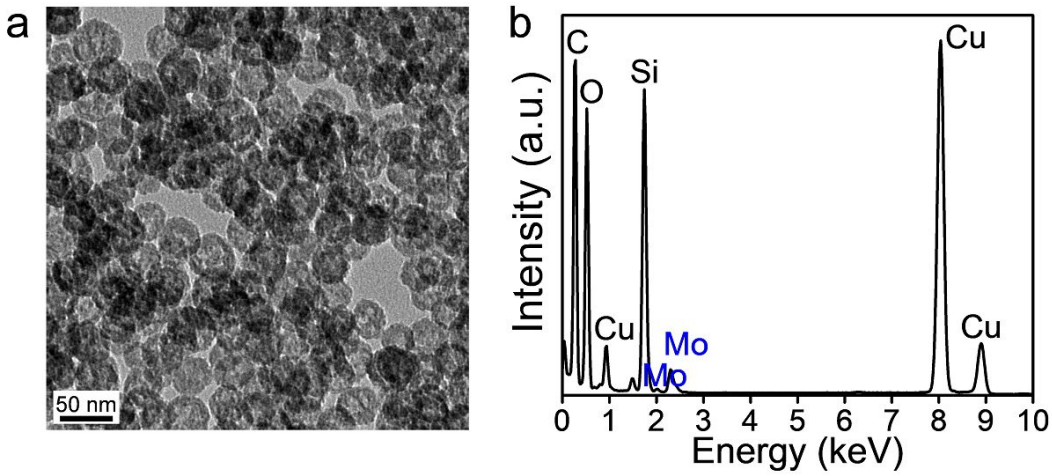

Figure S4. (a) High magnification TEM image and (b) EDS spectrum of HMOPM at pH 5.5 solution.

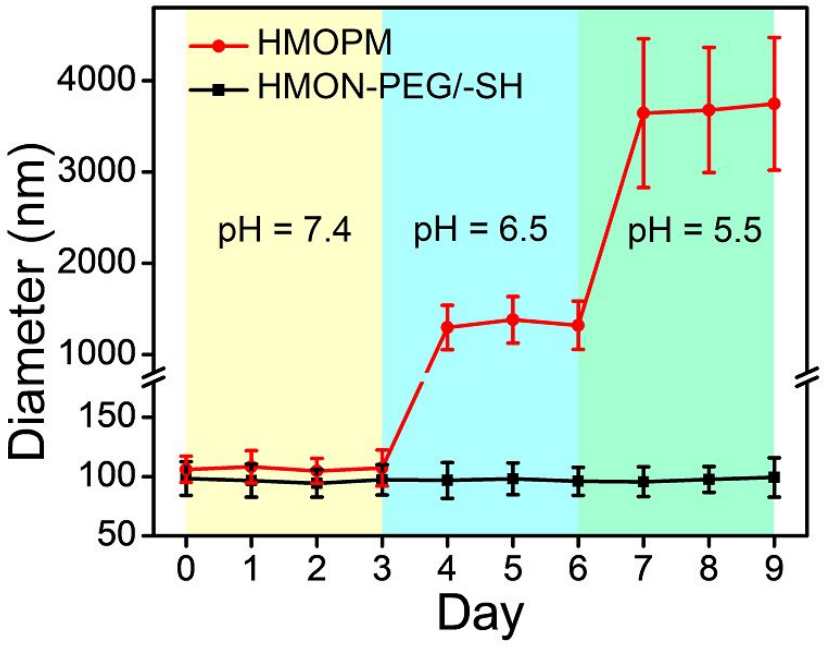

Figure S5. DLS measurements of HMOPM or PEG and thiol co-modified HMON (HMON-PEG/-SH) with successive acidifications from pH = 7.4 to pH = 5.5.

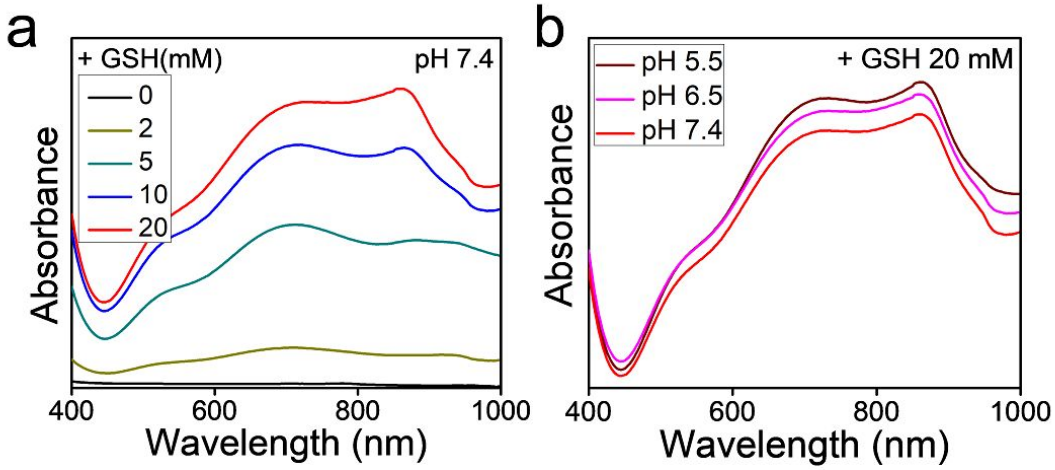

Figure S6. (a) UV-Vis absorption spectra of HMOPM solutions incubated with various concentrations of GSH (0, 2, 5, 10, 20 mM) at pH 7.4. (b) UV-Vis absorption spectra of HMOPM solutions incubated with 20 mM GSH at different pH values (7.4, 6.5, and 5.5).

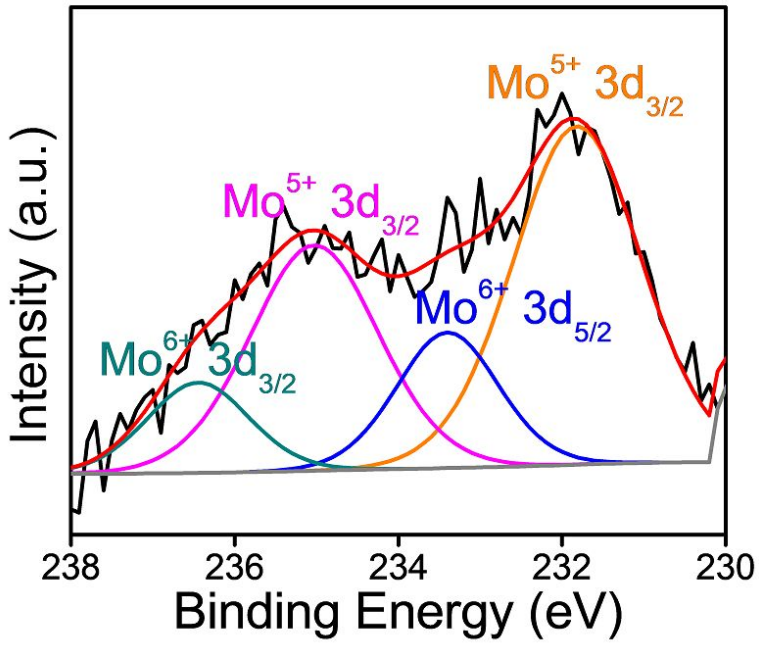

Figure S7. XPS spectrum of Mo 3d in HMOPM after incubation with 10 mM GSH. Part of Mo in HMOPM was reduced from VI to V oxidation state.

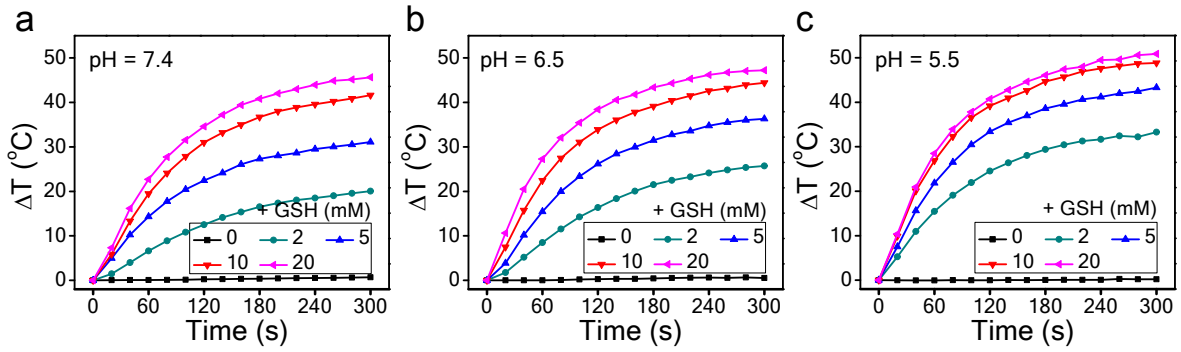

Figure S8. Photothermal heating curves of HMOPM aqueous solutions at various concentrations of GSH (0, 2, 5, 10, 20 mM) at (a) pH = 7.4, (b) pH = 6.5, and (c) pH = 5.5. An 808-nm laser irradiation at 1.0 W/cm^2 was applied. The temperature rise was found to be a function of the GSH concentration and the pH value of the solution.

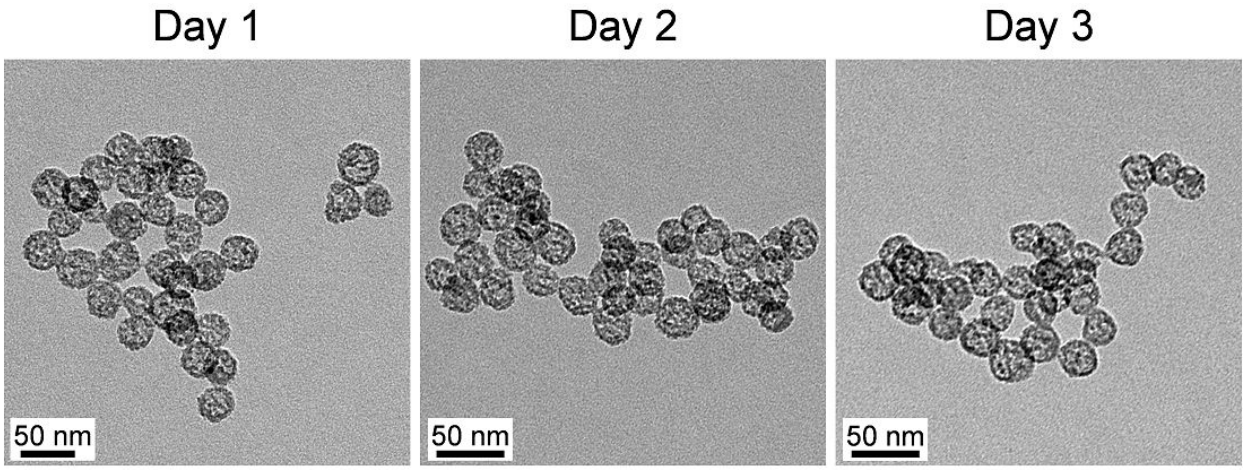

Figure S9. Stability test of HMOPM in reductive conditions at GSH concentration of 10 mM.

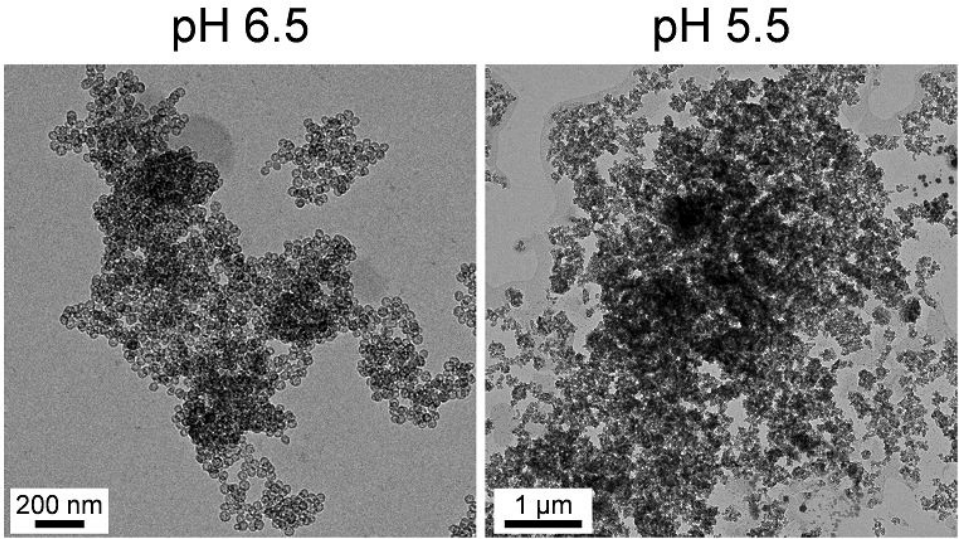

Figure S10. TEM images of GSH-reduced HMOPM at acidic solutions.

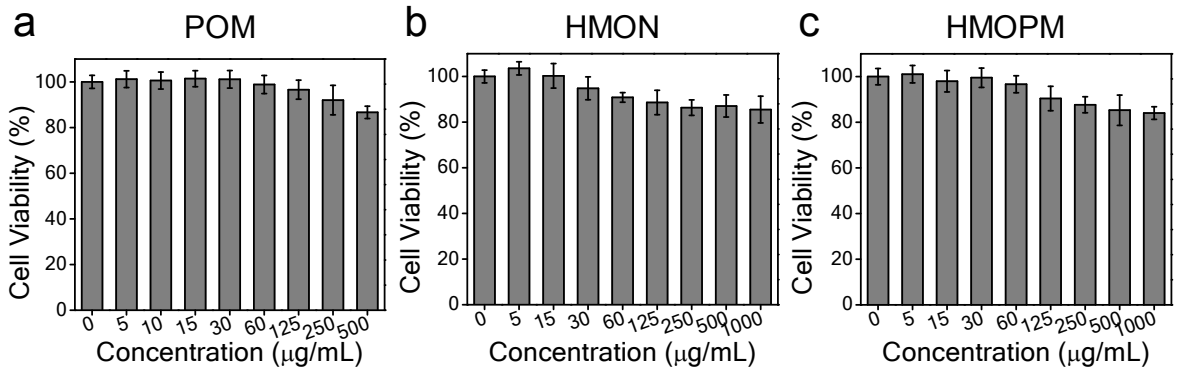

Figure S11. MTT assays on U87MG cells after 24 hours of co-incubation with (a) POM, (b) HMON, and (c) HMOPM at different concentrations. All these materials exhibited relatively high biocompatibility.

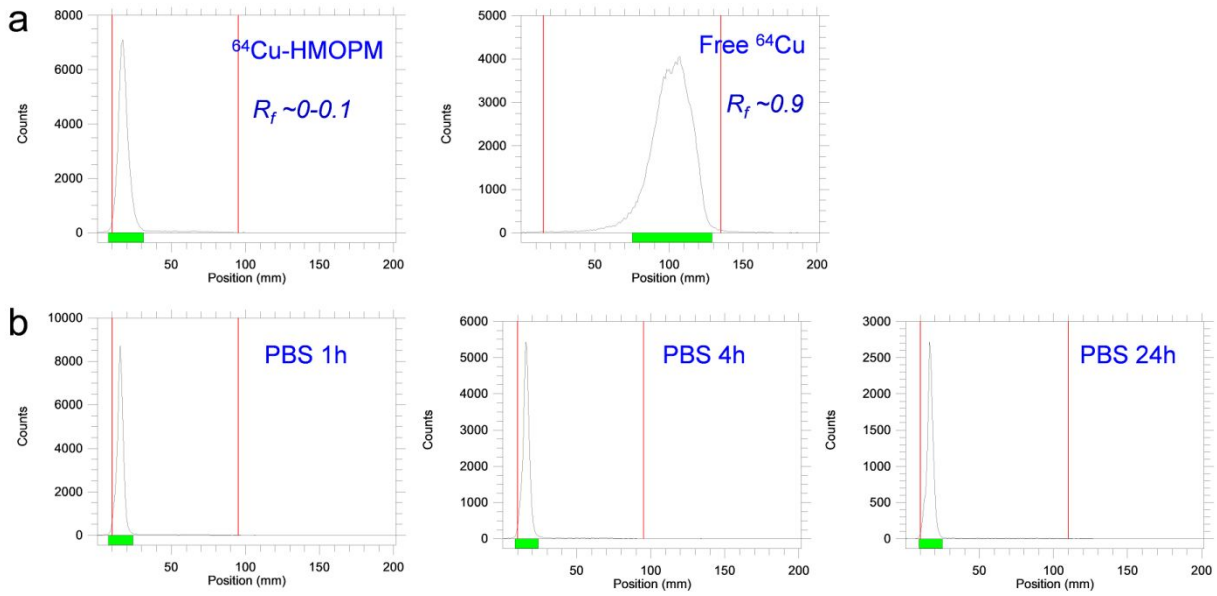

Figure S12. (a) Radio-TLC analysis on ^{64}Cu-labelled HMOPM (^{64}Cu-HMOPM) and free ^{64}Cu. (b) Radio-TLC analysis on ^{64}Cu-HMOPM after incubation in PBS for 1, 4, and 24 hours.

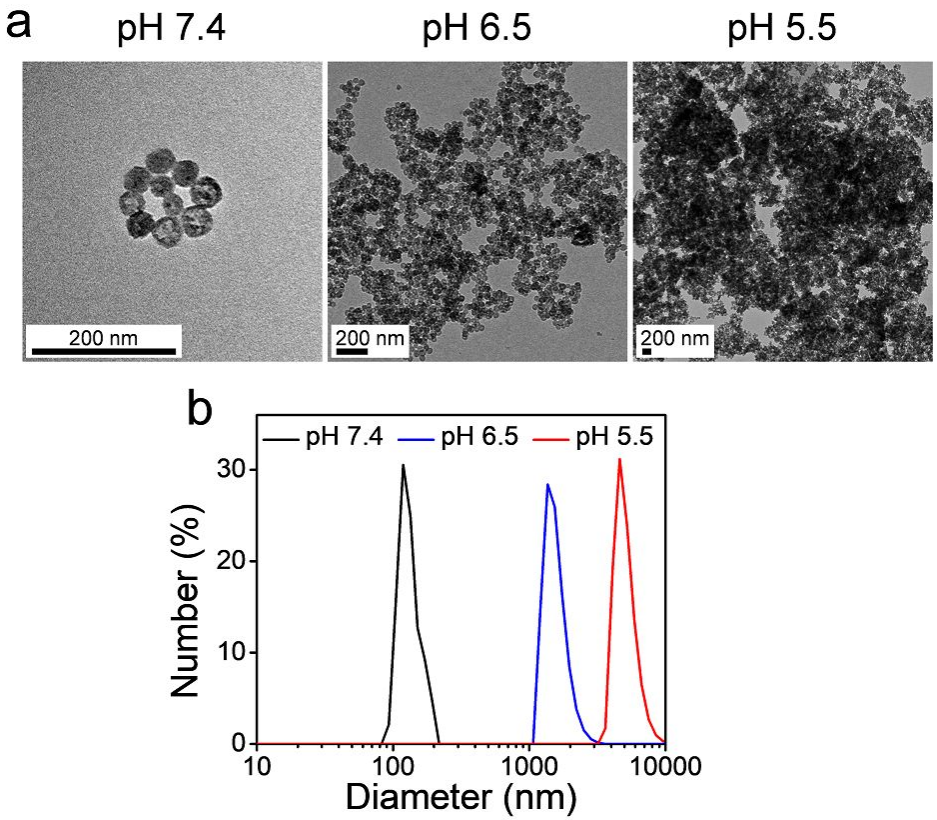

Figure S13. (a) TEM images of HMOPM-CO at different pH values. Scale bar, 200 nm. A low-acidity driven self-assembly of HMOPM-CO was observed. (b) Dynamic light scattering (DLS) size measurement of HMOPM-CO under different acidities corresponding to (a). The hydrodynamic sizes of HMOPM were determined to be 124.9 ± 13.7,1467.4 ± 285, and 4781.5 ± 882.6 nm with consecutive acidifications from pH = 7.4 to 6.5 and to 5.5.

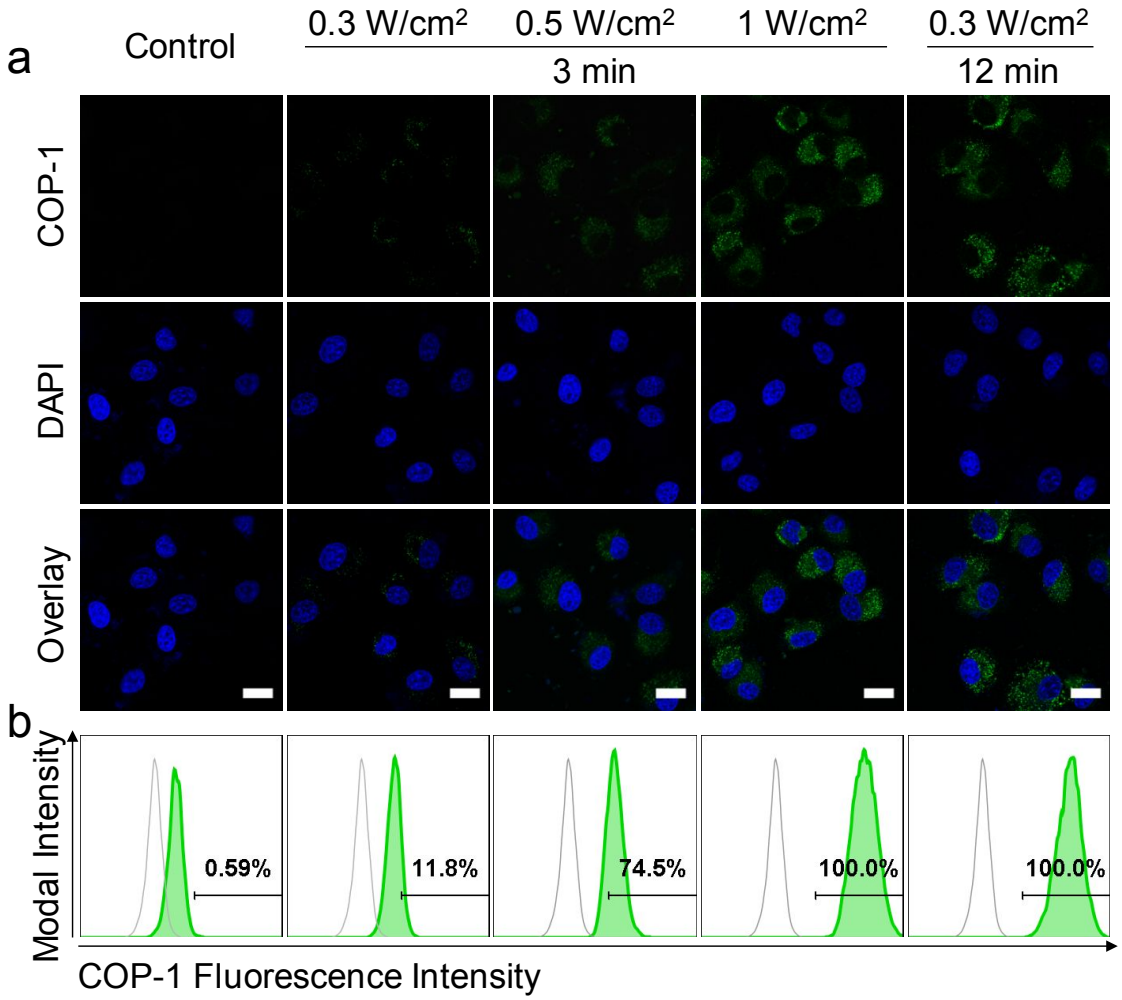

Figure S14. Intracellular CO release evaluation with the COP-1 probe. U87MG cells were treated with HMOPM-CO (GSH pre-incubated) plus an 808-nm laser irradiation at different fluences (0.3, 0.5, 1.0 W/cm^2). (a) Confocal microscopy analysis. When exposing the cells to an elevated irradiation fluence for the same duration, an intensified green fluorescence signal was observed, indicating elevated intracellular CO level. Moreover, the CO release amount was dependent on both the irradiation fluence and the irradiation time. Cells treated with irradiations of 1.0 W/cm^2 for 3 min and 0.3 W/cm^2 for 12 min induced similar level of extensive CO generation. Green, COP-1. Blue, DAPI. Scale bar, 20 μm. (b) Flow cytometry analysis validated the same positive correlation between the CO generation and irradiation fluence.

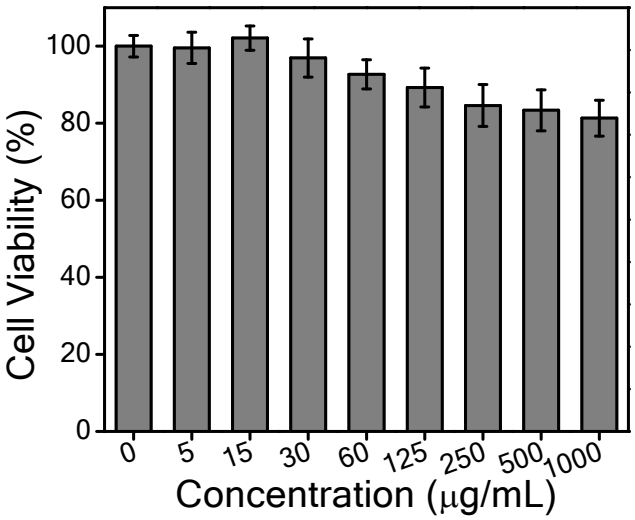

Figure S15. MTT assay on U87MG cells after 24 hours of co-incubation with HMOPM-CO. The HMOPM-CO demonstrated high biocompatibility.

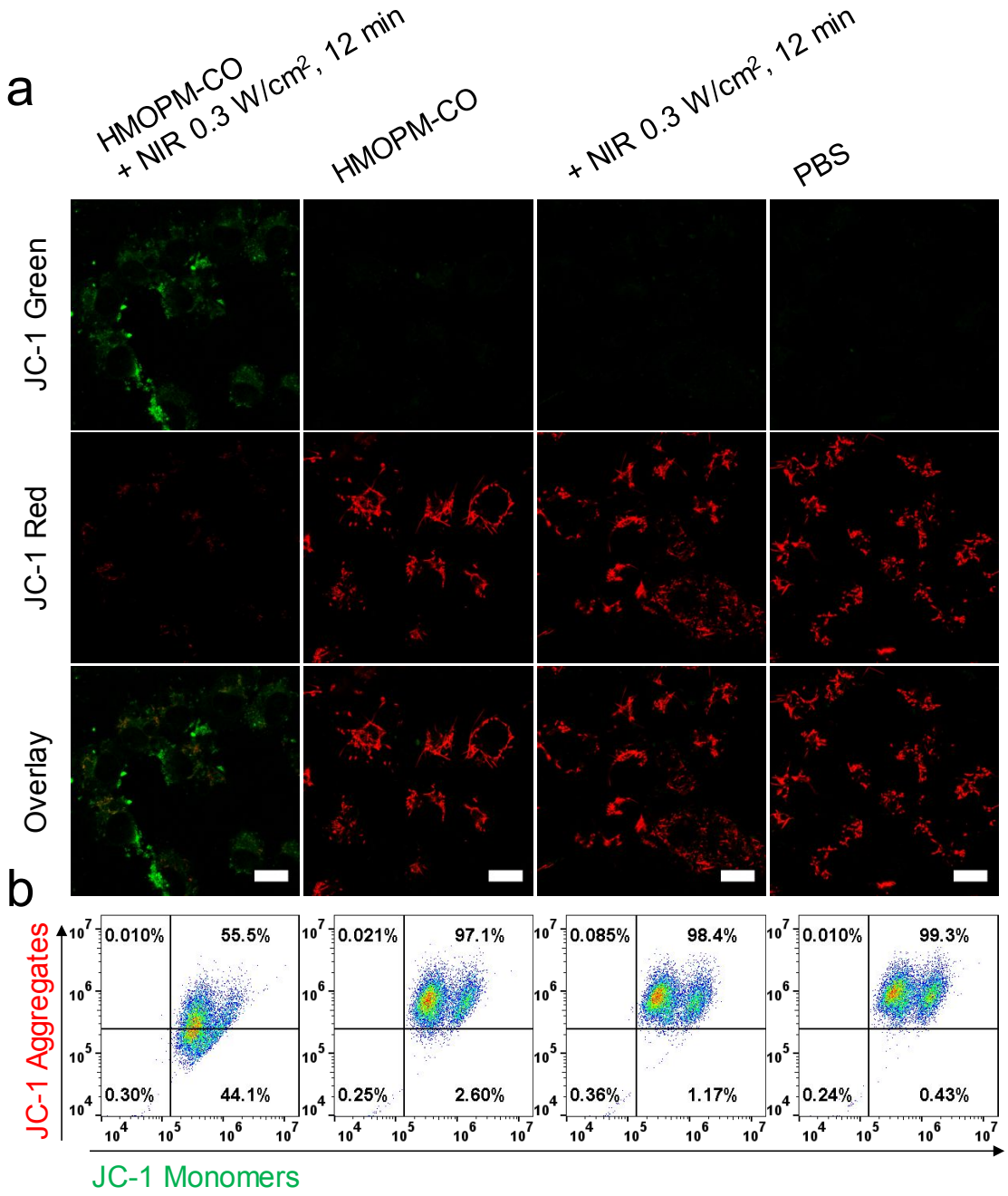

Figure S16. JC-1 assays on cells for evaluating mitochondrial membrane potential loss. Cells were treated with HMOPM-CO (GSH pre-incubated) and then exposed to an 808-nm laser at 0.3 W/cm^2 for 12 min. Cells treated with HMOPM-CO (GSH pre-incubated) only, NIR only, or PBS were set as controls. (a) Confocal microscopy analysis. Green, JC-1 monomers, low mitochondrial membrane potential. Red, JC-1 aggregates, high mitochondrial membrane potential. Scale bar, 20 μm. (b) Flow cytometry analysis on JC-1 fluorescence of cells after different treatments. Decreased red (JC-1 aggregates) to green (JC-1 monomer) fluorescence ratio were observed in the HMOPM-

CO plus NIR treated group, indicating damaged mitochondria resulted from the CO gas therapy. In contrast, all control groups exhibited overwhelming red fluorescence with negligible green florescence, suggesting a normal cellular polarization state.

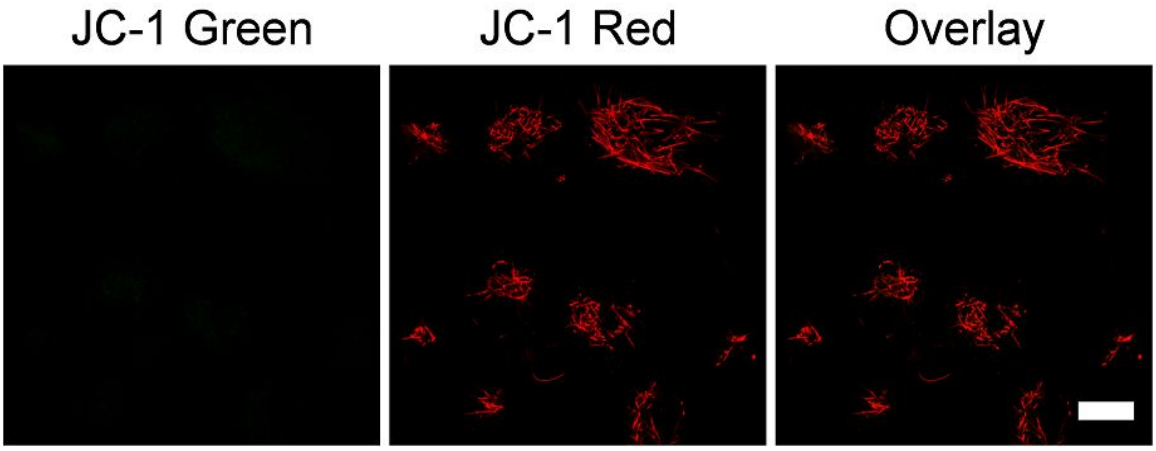

Figure S17. JC-1 assay on cells with mild hyperthermia treatment (HMOPM + 808-nm laser at 0.3 W/cm^2 for 12 min). Extensive red fluorescence was observed after the treatment, suggesting negligible damage on mitochondrial. Scale bar, 20 μm.

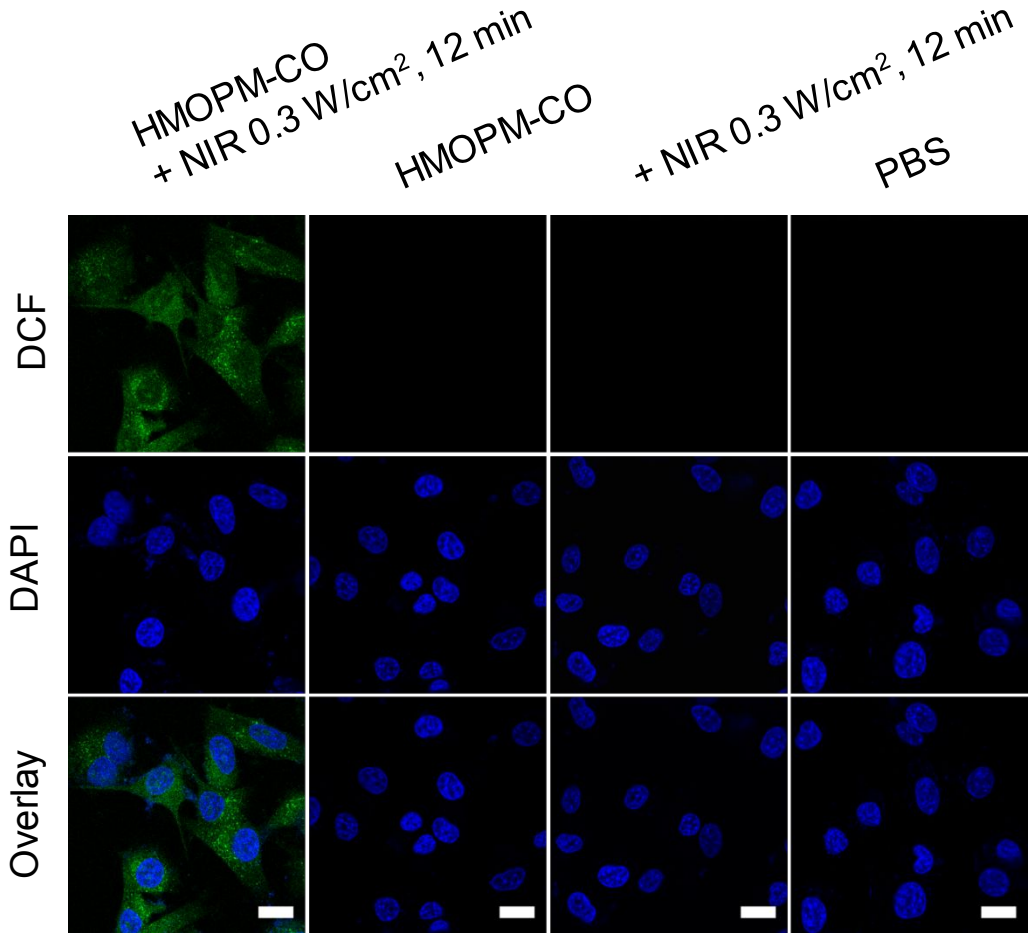

Figure S18. H_2DCFH-DA assays on cells for detecting ROS generation. Cells were treated with HMOPM-CO (GSH pre-incubated) and then exposed to an 808-nm laser at 0.3 W/cm^2 for 12 min. In the control groups, cells were treated with HMOPM-CO (GSH pre-incubated) only, NIR only, or PBS. An explosive green fluorescence was observed in the HMOPM-CO plus NIR treated group, suggesting elevated intracellular ROS level after the CO gas therapy. Green, DCF. Blue, DAPI. Scale bar, 20 μm.

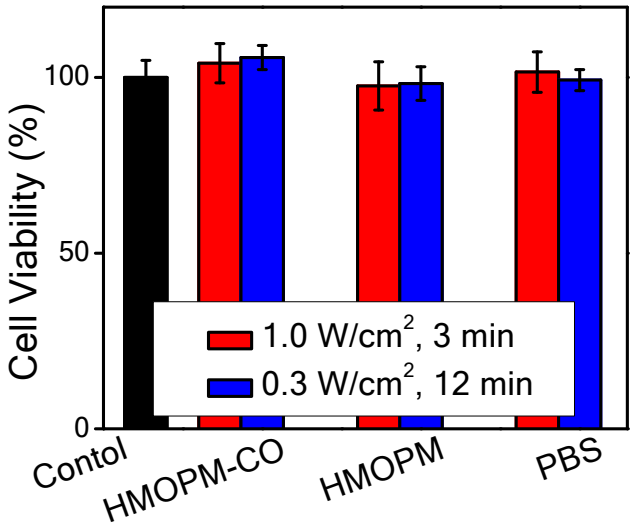

Figure S19. MTT assay on U87MG cells after 24 hours of an 808-nm laser irradiation (1.0 W/cm^2 for 3 min or 0.3 W/cm^2 for 12 min) with HMOPM-CO (without GSH pre-incubation), HMOPM (without GSH pre-incubation), or PBS. In the absence of GSH, the HMOPM-CO and the HMOPM at the highest oxidation state of Mo(VI) resulted in negligible phototoxicity, indicating highly tumor-selective photothermal agents *in vivo*.

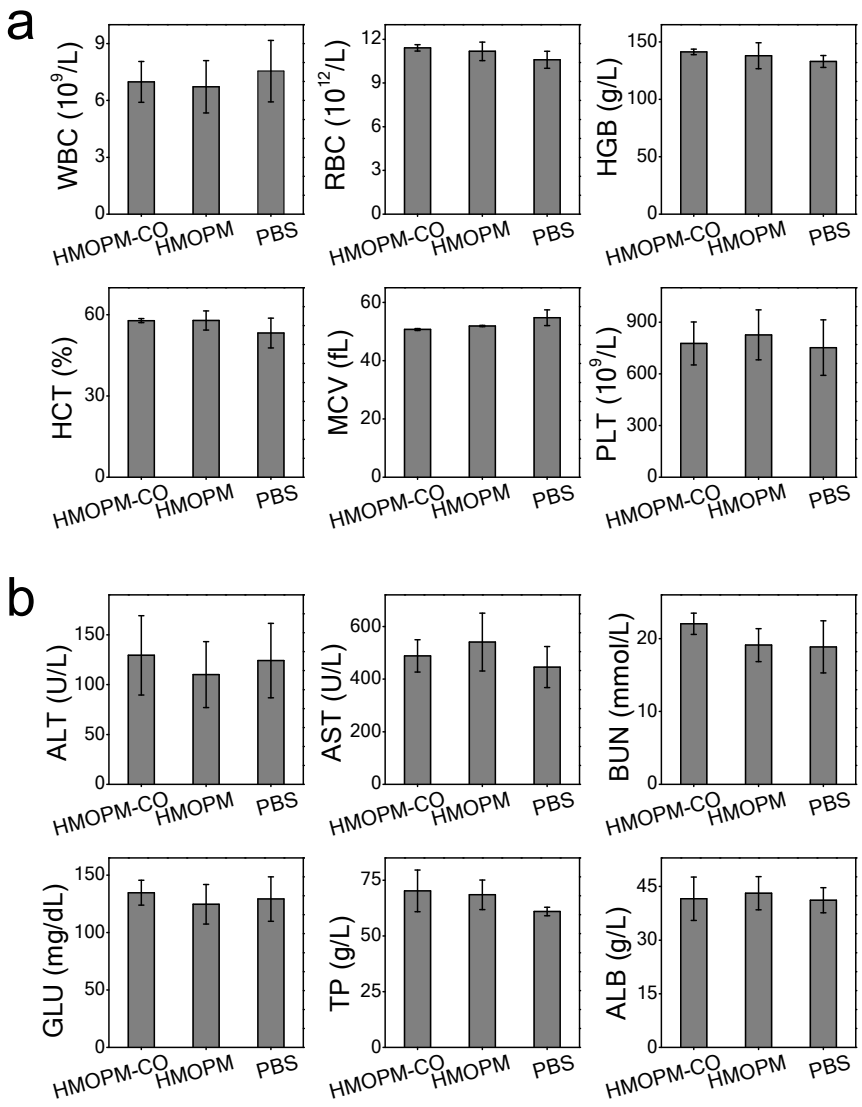

Figure S20. *In vivo* toxicity evaluation. (a) Hematological index and (b) biochemical blood analysis of the balb/c mice after 7 days of intravenous injection with the HMOPM-CO, the HMOPM, and PBS in separate groups.

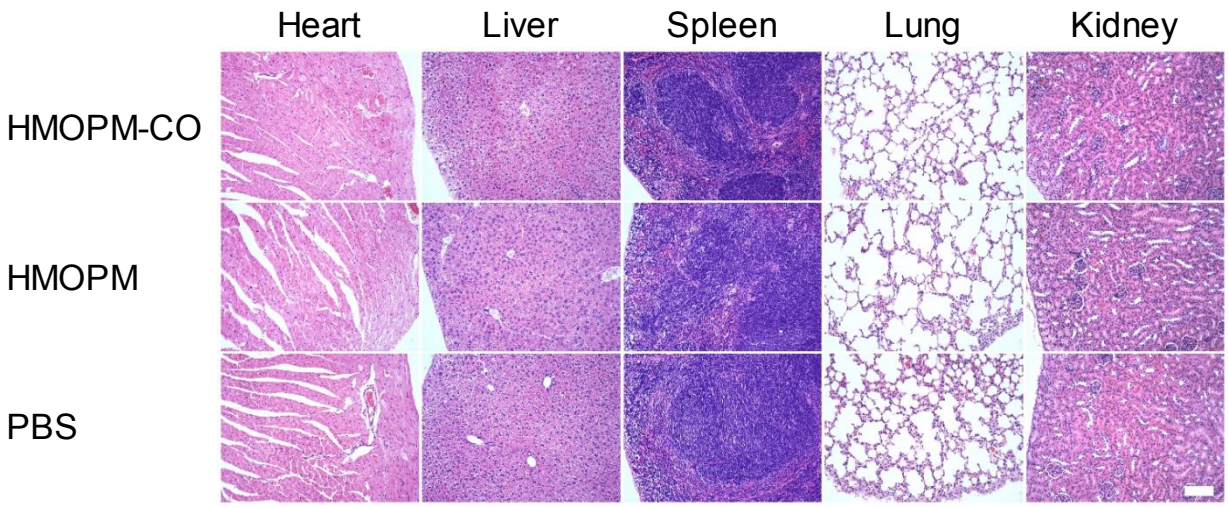

Figure S21. H&E staining on major organs (heart, liver, spleen, lung, and kidneys) of the HMOPM-CO, HMOPM, and PBS-treated balb/c mice at 7 days p.i. in separate groups. Scale bar, 100 μm.

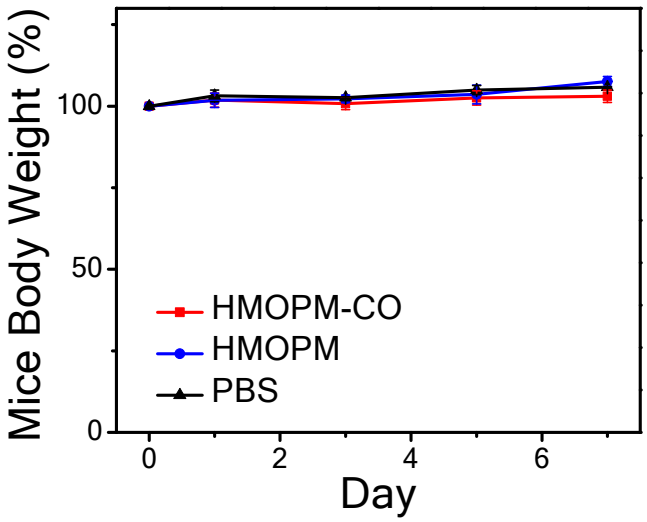

Figure S22. Body weight changes of balb/c mice after intravenous injection of HMOPM-CO, HMOPM, and PBS in separate groups.

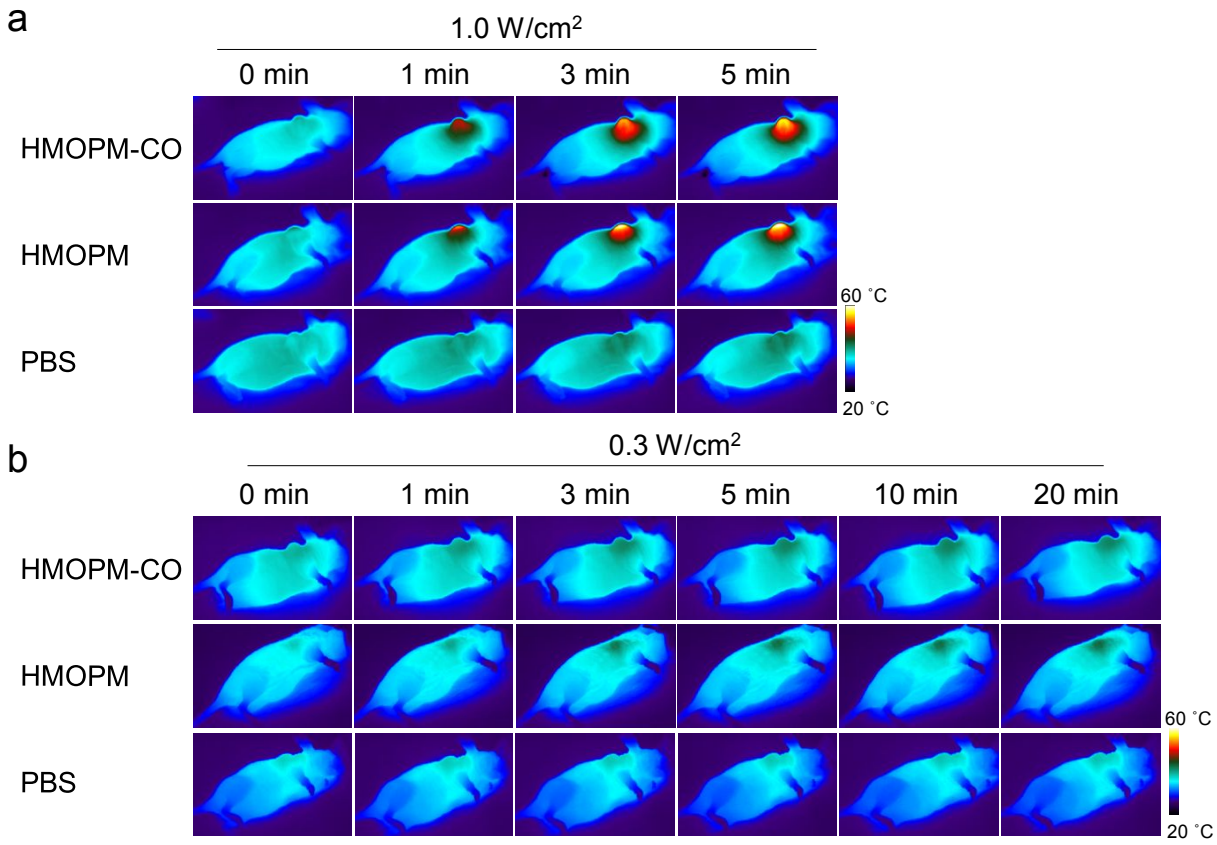

Figure S23. Thermographic images of mice treated with HMOPM-CO, HMOPM, or PBS in separate groups and then exposed to an 808-nm laser irradiation at (a) 1.0 W/cm^2 for 5 min or (b) 0.3 W/cm^2 for 20 min at 24 h p.i. Only a 1.0 W/cm^2 laser irradiation on the HMOPM-CO-treated or the HMOPM-treated tumors would give rise to photothermal killing effects.

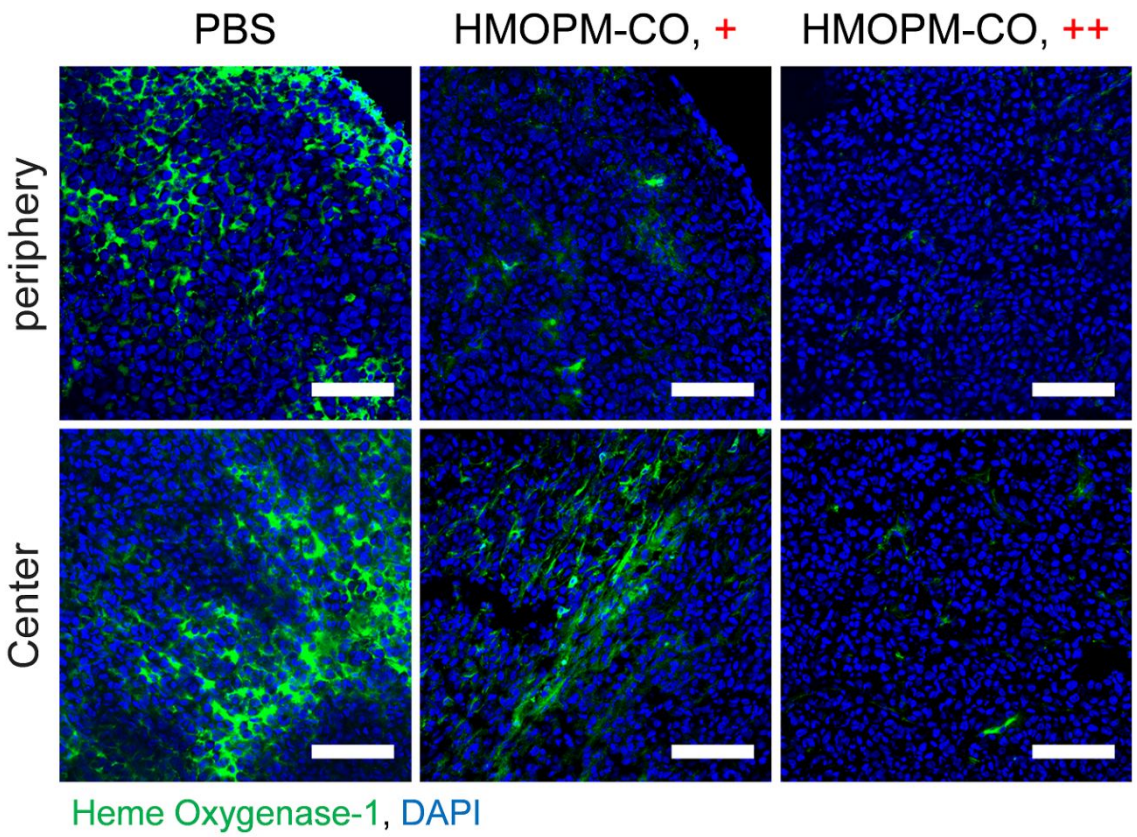

Figure S24. Immunofluorescence staining of heme oxygenase-1 (HO-1) after treatments. The HO-1 expression can be downregulated by CO released from CO-releasing molecules. "+" stands for an 808-nm NIR irradiation at 0.3 W/cm^2 for 20 min. "++" stands for an 808-nm NIR irradiation at 1.0 W/cm^2 for 5 min. With a mild hyperthermia (HMOPM-CO, +), a significant fluorescence signal drop was observed only at the periphery but not the center of tumors, which may because most nanoparticle aggregation and CO release happened at the outside layer of solid tumor. However, a high photothermal temperature (HMOPM-CO, ++) could accelerate the release and diffusion of CO in tumors, showing greatly suppressed HO-1 expression in the center of the tumor as well. Green, HO-1. Blue, DAPI. Scale bar, 100 μm.

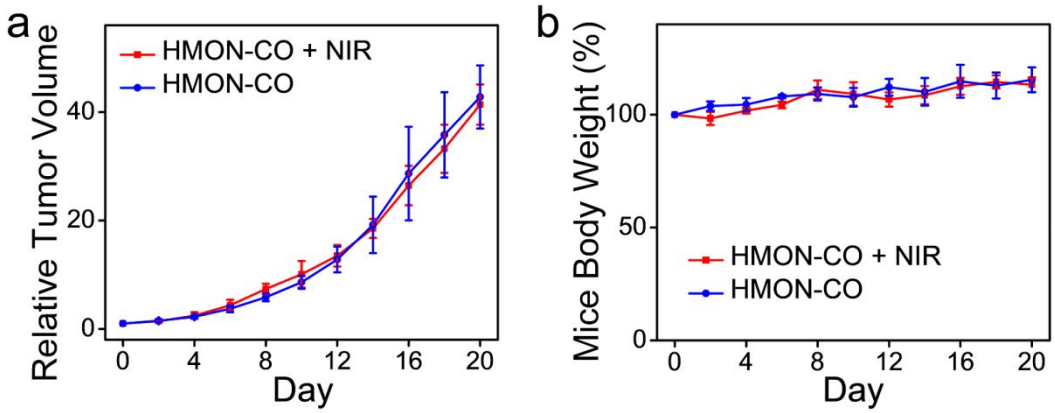

Figure 25. Therapy studies with $Mn_2(CO)_{10}$-loaded and PEG-modified HMON (HMON-CO) or HMON-CO with an NIR irradiation (808 nm, 1 W/cm^2, 5 min). (a) Tumor growth curves. (b) Mice body weight change curves.

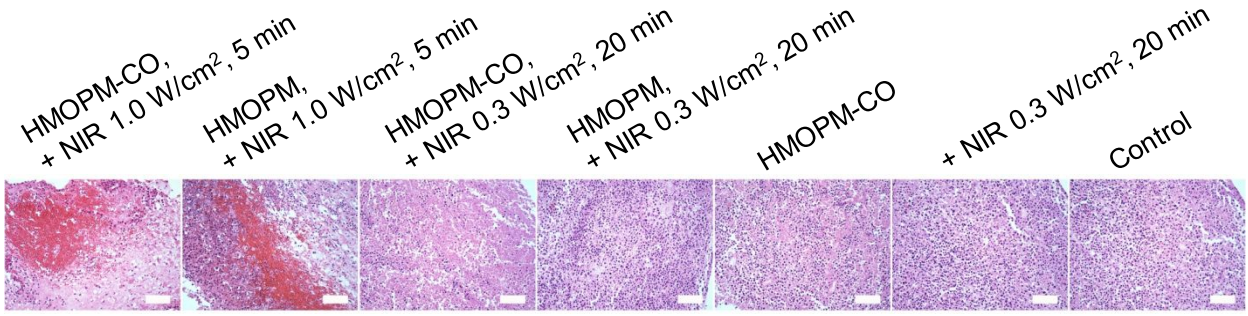

Figure S26. H&E staining on tumor samples acquired after 24 hours of different treatments. H&E staining images revealed extensive cell necrosis and severe disturbed tumor structures in the tumors treated with PTT and/or gas therapy. Large bleeding regions were found in PTT-involved treatment groups, suggesting effective synergistic PTT-enhanced CO gas therapy. Scale bar, 100 μm.

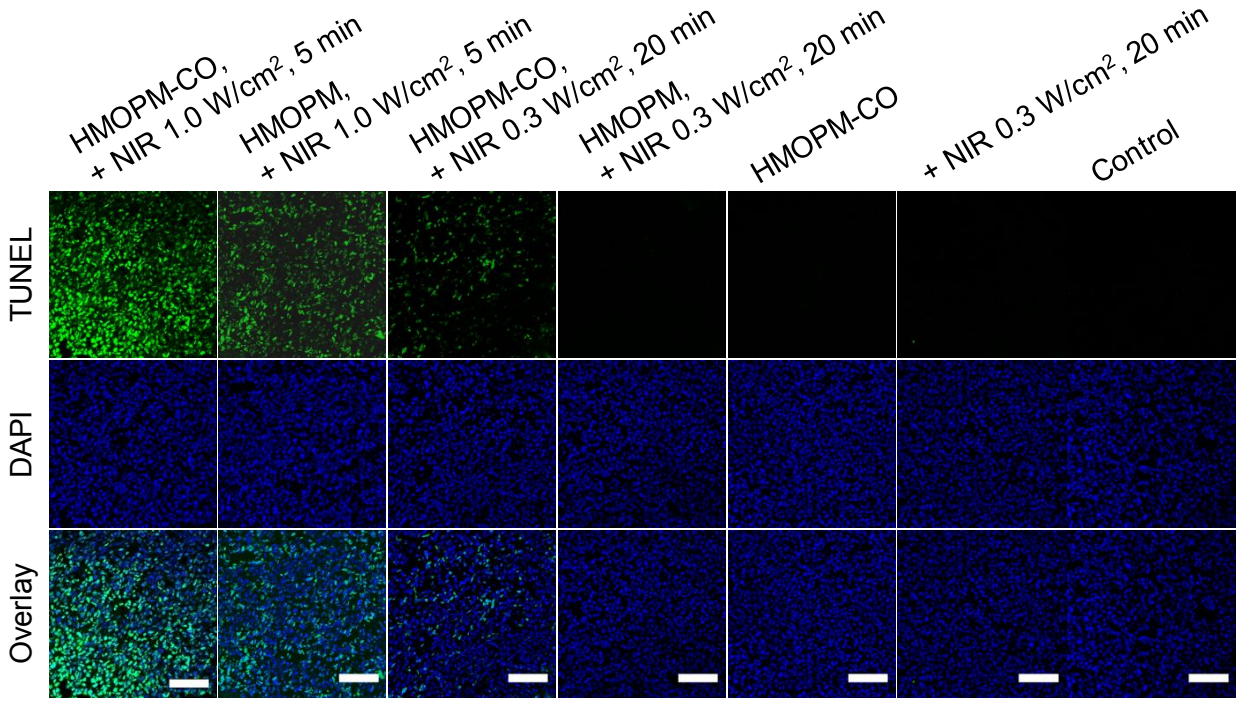

Figure S27. TUNEL assay performed on tumor samples acquired after 24 h of different treatments. An explosive level of green fluorescence was observed in the PTT-enhanced CO gas therapy group, indicating wide spread apoptotic cells after the synergistic treatment. Green, TUNEL. Blue, DAPI. Scale bar, 100 μm.

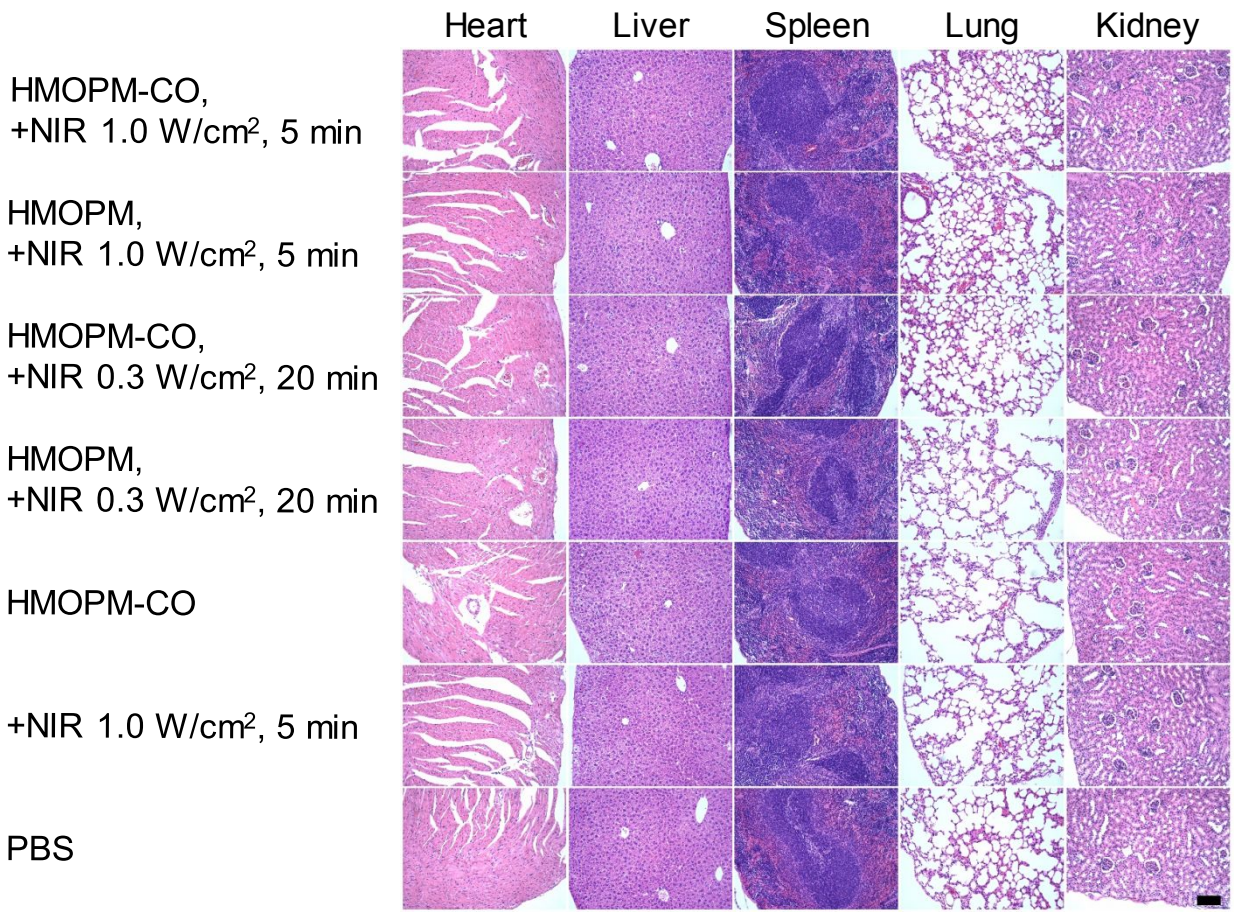

Figure S28. H&E staining on major organs (heart, liver, spleen, lung, and kidneys) at the end of the therapy studies. No obvious pathological abnormalities were observed. Scale bar, 100 μm.

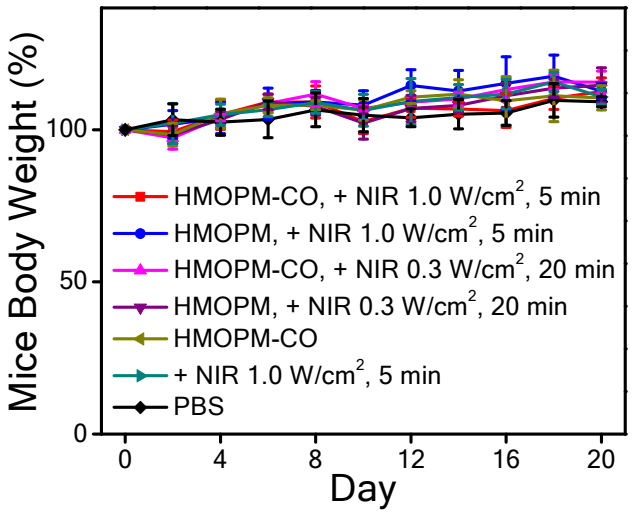

Figure S29. Mice body weight changes during the therapy studies. No significant mice body weight drops were observed, suggesting little side effects caused by the treatments.